IEEE Access
Multidisciplinary | Rapid Review | Open Access Journal

Received June 25, 2019, accepted July 2, 2019, date of publication July 9, 2019, date of current version July 26, 2019.

Digital Object Identifier 10.1109/ACCESS.2019.2927615

A New Vibration Device Applied for Two-Dimensional Ultrasonic Polishing of Biomaterials

JIEQIONG LIN[1], HAO LU[1], YAN GU[1], XIAOQIN ZHOU[2], CHENGLEI XIN[1], MINGSHUO KANG[1], AND XINYU CANG[1]

[1]Key Laboratory of Micro-Nano and Ultra-Precision Manufacturing of Jilin Province, Mechatronic Engineering Department, Changchun University of Technology, Changchun 130012, China
[2]School of Mechanical and Aerospace Engineering, Jilin University, Changchun 130022, China

Corresponding author: Yan Gu (guyan@ccut.edu.cn)

This work was supported in part by the National Ministry of Science and Technology International Cooperation Project under Grant 2016YFE0105100, in part by the Micro-Nano and Ultra-Precision Key Laboratory of Jilin Province under Grant 20140622008JC, and in part by the Science and Technology Development Projects of Jilin Province under Grant 20180623034TC and Grant 20190201254JC.

ABSTRACT For the research of the performance of two-dimensional ultrasonic polishing (TDUP) on the biomaterials, a new vibration device was designed. Meanwhile, our aim is to study the mechanism of multiangle polishing to cope with the complex structure of biomaterials. The device is composed of piezoelectric rings, asymmetric transformer, ultrasonic generator, and so on. The structural dimension parameters were optimized by finite element analysis, and especially the groove size on the transformer was discussed in detail. Two kinds of experiments had been conducted to test the performance of the proposed device, including impedance analysis experiments and amplitudes measurement experiments. Furthermore, a mechanical model to explain the principle of the multiangle polishing was set up, which could assist to analyze the influence of different polishing angles in terms of machining. Finally, the machining experiments and multiangle polishing experiments were carried out to verify the effectiveness of the device. Compared with traditional mechanical polishing, the surface roughness is reduced from 235 nm to 140 nm. The results of multiangle polishing experiments indicate that the surface quality of biomaterials will be prominently affected by different polishing angles. In addition, the polishing mechanism will transform owing to the inversion of the normal velocity during the polishing process with the angle increasing. The surface morphology will also be affected. It has been proven that the experimental results agree with the model well.

INDEX TERMS Vibration device, multiangle polishing, two-dimensional ultrasonic vibration, biomaterials.

I. INTRODUCTION

Biomaterials possess superior biocompatibility, tough strength and excellent corrosion resistance, which arouse wide attentions from researchers in recent years. The modern biomaterials have been extensively utilized in the medicine throughout dental implants, fracture treatment, joint replacement, and spinal surgery based on materials performance improvement [1]. Nevertheless, it is inevitable fact that most of them are difficult-to-machine materials and the quality of medical products are required to further polish to acquire high surfaces quality. While the traditional mechanical polishing methods hardly arrive the precise surfaces under adverse working conditions, such as small area with complex structure. Improving surface quality and prolonging service life, many researches have been conducted on biomaterials which covered titanium alloy, nickel-based alloy, and ceramics. The premature failure of materials (e.g., fractured, loosened, and deformation) can severely degrade their strength and life, which will induce serious consequences. Therefore, it is a huge challenge to discover an efficient and high-quality polishing method for the preparation of biomaterials.

Ultrasonic assist machining is famous for the typical intermittent machining principle that the tool has a contact-separation process in a cycle. High frequency periodic separation has the advantages of small average force,

The associate editor coordinating the review of this manuscript and approving it for publication was Yuhao Liu.

high efficiency and high surface quality [2], [3]. The researches on ultrasonic machining cover wide ranges, such as the problem of the boundary damage of rotary ultrasonic machining [4], the investigation on machining performance of two-dimensional ultrasonic machining [5], the separation phenomenon of ultrasonic machining [6], and the application of anti-counterfeiting of surface microstructure through by two-dimensional ultrasonic machining [7]. Moreover, researchers have also done a number of studies on ultrasonic polishing. It can significantly improve the surface quality and the material removal rate (MRR) of workpiece. Yu et al. used one-dimensional ultrasonic vibration combining with ultrasonic atomization suspension method for polishing the nickel-based alloy and established MRR model of polishing. The experimental results demonstrate that the method is able to reduce the roughness of the machined surface and improve the MRR according to the quantitative analysis [8]. In the subsequent study, they investigated the ultrasonic vibration-assisted polishing on Mono-crystalline silicon and utilized the molecular dynamics simulation (MDS) to explain the effect of ultrasonic vibration on the MRR and surface quality. A MRR model of single abrasive was developed and polishing experiments were conducted. The results reveal that ultrasonic polishing can significantly improve the MRR and obtain better surface quality compared to the conventional mechanical polishing [9]. Xu et al. performed ultrasonic flexural vibration assisted chemical mechanical polishing on the sapphire substrates. Then, the surface morphology and MRR were observed. Experimental results show that the MRR of the composite polishing method is twice as much as conventional chemical polishing. And the surface roughness ranges from 0.212nm to 0.083nm. It has been proved that the composite polishing method can improve the MRR and surface quality of sapphire substrate [10]. However, those studies above lack a solution for small areas with specific structures. H. Suzuki et al. utilized one-dimensional ultrasonic device to polish binder-less tungsten carbide to meet the requirements of smaller aspheric lenses and higher precision. The experimental results show that the PV value of the surface could reach 70nm and the surface roughness could reach 7nm [11]. Later, an ultrasonic two-axis vibration assisted polishing machine was introduced into finishing the molds to improve the accuracy. Polishing experiments were carried out on binder-less tungsten carbide molds. The experimental results demonstrate the surface roughness of 8 nm Rz is obtained [12]. Zhao et al. investigated micro cylindrical SiC surface of ultrasonic vibration assisted polishing. The friction behavior on SiC cylindrical surface was analyzed by the collection method of high frequency friction forces. The removal methods under different polishing parameters are also explained. The results show that the surface roughness of SiC microcylinder is lower and the polishing marks are less because the lower polishing force, polishing speed and higher vibration frequency, amplitude [13]. Hocheng et al. developed a novel ultrasonic polishing system for the mold steel polishing experiments. In addition, the path was planned to cover the entire surface. The effects of abrasive particle size and static load on surface finish were studied. The optimum abrasive size was determined. Experimental results reveal that large static load could achieve effective polishing [14]. This kind of polishing form is benefit for precise polishing of small area with complex structure.

Ultrasonic assisted machining has been applied in biomaterials for its excellent machining performance in difficult-to-machine materials. Jia et al. combined two-dimensional ultrasonic vibration with nanofluid minimum quantity lubrication (NMOL) technology for grinding medical zirconia ceramics. The study shows that the approach can improve the adhesion and materials peeling phenomenon and reduce the surface roughness of zirconia materials [15]. Zheng et al. conducted the studies of titanium alloy by rotary ultrasonic milling. The surface friction and wear were tested by adjusting ultrasonic power and pre-pressure. The results indicate that the surface quality of workpiece decrease due to the parameters are out of range and the neat microstructures are destroyed [16]. Xiao et al. processed zirconia ceramics by rotary ultrasonic milling. Considering the influence of overlapping and crossing of active abrasive particles in fracture zone on cutting force, a mechanical model was established. The experiments about the relationship among cutting force, spindle speed, feed, cutting depth and other variables were carried out. The results indicate that the mechanical model can provide reference for the efficient machining of zirconia ceramics by rotary ultrasonic milling [17]. Pujana et al. applied ultrasonic vibration on the drilling of Ti6Al4V workpiece samples for researching the relationship of parameters including feed force, chip formation, and temperature. The results show that lower force and higher temperatures are obtained compared with conventional drilling. It has been observed that there are higher force reductions and higher temperature increments as the increasing of vibration amplitudes [18]. It is relative remarkable that the ultrasonic researches on biomaterials are mostly ultrasonic drilling, ultrasonic milling, and there are not enough evidences on two-dimensional ultrasonic polishing of the biomaterials. Compared to one-dimensional ultrasonic vibration, two-dimensional ultrasonic vibration has completely separated from the workpiece surface in each cycle, which has smaller average force, easier chipping and lower temperature in the processing area [19]. The surface with vibration structure produced by TDUP have a three-dimensional structure that may facilitates the attachment of human cells and tissues on the implant. Therefore, the research on the TDUP of biomaterials is of great significance [20].

In recent years, two-dimensional ultrasonic devices have been continuously developed. At present stage, two-dimensional ultrasonic device mainly includes three ideas for design. One is a longitudinal vibration piezoelectric rings driven by single AC signals to generate two-dimensional ultrasonic vibration due to its special transformer structure [21], [22]. The second is that a couple transducers at a certain angle are excited to produce two-dimensional

ultrasonic vibration [23], [24]. The third is that single AC signals drive the piezoelectric rings of the longitudinal and the bending vibration to form two-dimensional ultrasonic vibration [25], [26]. In addition, there are some ultrasonic devices with specific functions [27], [28], [29]. It is noteworthy that the employed two-dimensional ultrasonic device for polishing biomaterials also could be adjusted for applications. For example, substitutes of human skeleton with complex structural surfaces are typical biomedical products. It is inevitable that the machine angle will change during the machining of some complex surfaces, which leads to diversity in the surfaces quality of biomaterials. However, the previous ultrasonic devices have certain limitations and cannot be directly utilized for TDUP of biomaterials. Thus, the device should be accommodated to this situation of the changes of polishing angle. Researchers in the field of two-dimensional ultrasonic machining have studied the effects of machine angle. On the one hand, the machine angle is obtained by adjusting the angle between a couple transducers, with the phase difference being invariant [15]. On the other hand, the machine angle is obtained by changing the phase difference, with the included angle being invariant [23]. However, these methods not only change the machine angle relative to the workpiece surface, but also the movement trajectory and machining time. More detailed researches about angle should be conducted to initiatively adapt to the biomaterials processing.

According to the description above, a multiangle TDUP device has been applied to biomaterials is proposed to enrich the application fields of the two-dimensional ultrasonic device. Compare to the previous ultrasonic devices, the TDUP device proposed in this paper not only has obvious differences in the method of ultrasonic polishing, but also adapts to the change of machine angle. In addition, the design of rotary function further supports to study the effects of polishing angle on surface quality of biomaterials and fits the machining problems of complex surfaces. The model of multiangle is developed in order to analyze the effects more accurately and ensure the best strategy could be used in the actual polishing of biomaterials with complex surfaces in the future.

II. DESIGN OF DEVICE

A. COMPOSITION OF ULTRASONIC VIBRATOR

As shown in Fig. 1(a), ultrasonic vibrator consists of asymmetric transformer, transducer, back mass and some connectors. The ultrasonic vibrator is clamped by the bolt. Fig. 1(b) shows that the piezoelectric rings are polarized along thickness direction, which are arranged in mechanical in series and electrical in parallel. PZT-8 is selected. The clamped transducer is driven by AC signals at the resonant frequency of TDUP system and the piezoelectric rings produce high frequency vibration owing to the inverse piezoelectric effect. The vibration is transmitted and magnified by the asymmetric transformer which leads to the motion of polishing tool along elliptical trajectory. Meanwhile, the preload applied on the PZT rings can adjust the damping ratio of the structure that affects the vibration amplitudes. And the flange is exerted to connect the shell and its position is scheduled at the vibration node to avoid the adverse fixed impact. The length of the main parts of the ultrasonic vibrator (transformer, transducer, back mass) are calculated according to the design principle of one-dimensional ultrasonic vibrator, and the total length is one half of the wavelength. The thickness and radius of piezoelectric ceramics are known.

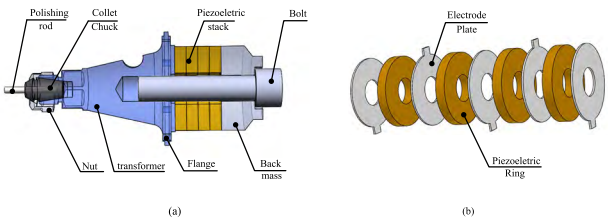

FIGURE 1. Schematic diagrams of ultrasonic vibrator (a) Components (b) Layout of piezoelectric ceramic rings.

B. FEM OF DEVICE

The finite element method (FEM) is utilized to optimize the structural parameters for improving the performance and recognizing the different vibration modes of the device. The 3D model is imported into ANSYS software and modal analysis and harmonic response analysis are applied. Material properties are listed in TABLE 1. Fixed constraint is set at the flange and 10N force is applied to polishing tool. In addition, the influence of electrodes is ignored in the simulation.

TABLE 1. Material properties of ultrasonic system components

Item	Materials	Young's Modulus (Pa)	Poisson's ratio	Mass Density (kg/m^3)
Transformer	TC4	1.15×10^{11}	0.310	4.43×10^3
Back mass	40Cr	2.11×10^{11}	0.277	7.87×10^3
Bolt	25Cr2MoV	2.11×10^{11}	0.300	7.62×10^3
Collet chuck	Cr12MoV	2.18×10^{11}	0.280	7.85×10^3
Nut	Cr12MoV	2.18×10^{11}	0.280	7.85×10^3

The lengths of each part are adjusted by modal analysis to determine the resonant frequency of longitudinal-bending mode. Fig. 2(a) is a schematic diagram of the modal analysis results of TDUP device. The result reveals that a two-dimensional ultrasonic vibration trajectory is obtained at 18661Hz frequency in the 14th mode. The (b), (c), (d), (e) represent the vibration position at different times in the same period. The movement of red marks along the orthometric arrows represents X- and Z-component of vibration respectively and the simulation pictures show the vibration state at the corresponding time. It can be clearly seen from these pictures that the tool part of the ultrasonic device vibrates to different positions.

The results of harmonic response analysis of ultrasonic vibrator are shown in Fig. 3. It shows the displacement curves

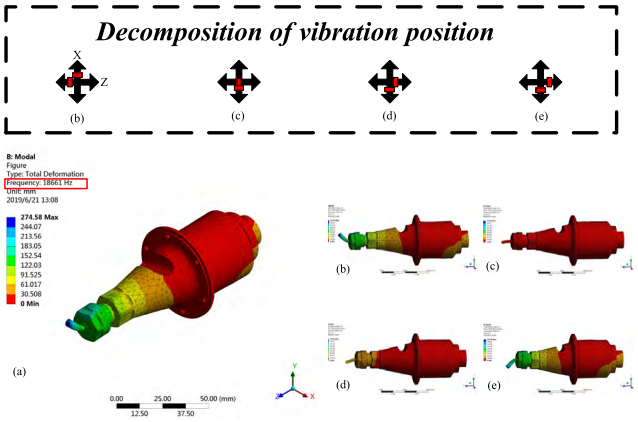

FIGURE 2. Vibration position of device at resonant frequency.

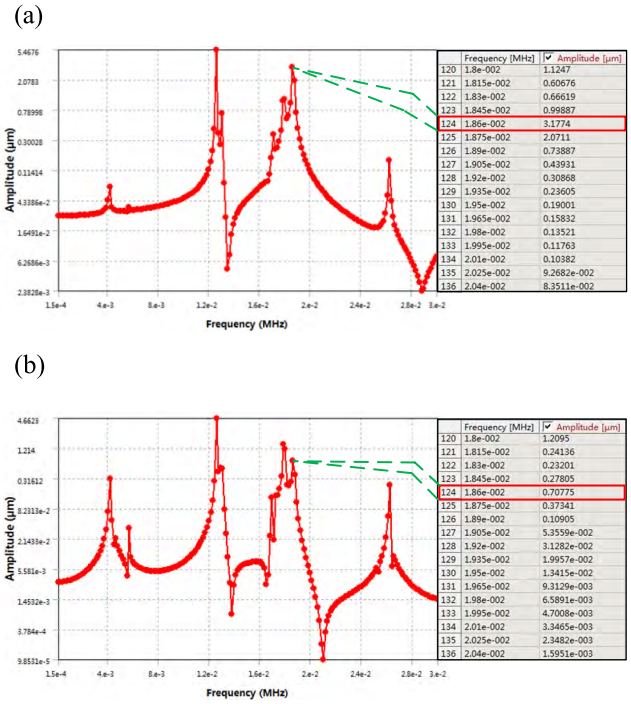

FIGURE 3. Amplitudes of *Z*- and *X*-directions of ultrasonic device (a) *Z*-direction (b) *X*-direction.

from 0 to 30kHz in the *Z*- and *X*-directions. The amplitudes corresponding to the resonance frequency obtained from the modal analysis is marked in red frames. Fig. 3(a) and Fig. 3(b) show the vibration amplitudes along *Z*-direction and *X*-direction are 3.18μm and 0.71μm, respectively, at the resonance frequencies of both 18661Hz. The ratio of amplitudes is 4.48. The results show that the vibration amplitudes of ultrasonic vibrator can be obtained by harmonic response analysis at the resonance frequency.

The conical transformer is employed and there is a groove on the transformer to form the asymmetric structure. The size of the groove determines whether ultrasonic vibrator can generate two-dimensional ultrasonic vibration. If the groove size is unsuitable (too small or big), it will make it hard to

TABLE 2. The sizes of the optimized ultrasonic vibrator

Item	Length (mm)	Diameter (mm)
Transformer	60	34 ; 20
Piezoelectric rings	4×5.5	Φ 15 ; D 40
Back mass	19.5	40 ; 30
Bolt	8.3	18
Polishing tool	10	3
Nut	11	19

generate two-dimensional ultrasonic vibration at the desired frequency range in the modal analysis. It is secure that we chose three typical kinds of grooves whose radius were 5mm, 8mm, 10mm, respectively. Modal and harmonic response analysis are conducted to these asymmetric transformers subsequently. Fig. 4 shows the modal simulation results when the grooves are different sizes on the transformer. It can be seen that the resonance frequencies of two-dimensional ultrasonic vibration generated by different grooves are significant differences. Fig. 4(a), Fig. 4(b) and Fig. 4(c) show that the ultrasonic vibrators in which the groove sizes are 5mm, 8mm and 10mm generate two-dimensional ultrasonic vibration with the resonant frequencies of 18661Hz, 18382Hz and 18050Hz, respectively.

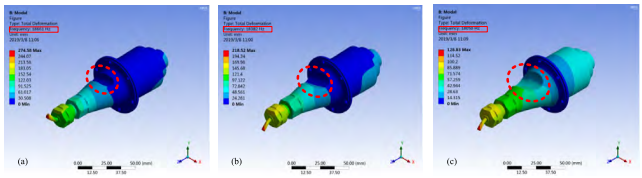

FIGURE 4. Modal analysis of different groove sizes (a) 5mm, (b) 8mm, (c) 10mm.

Fig. 5 demonstrates the influence of the groove sizes on ultrasonic amplitudes and resonance frequency in the simulation. Both the resonance frequency and amplitudes decrease with the increase of groove sizes. Ensuring higher resonance frequency and higher vibration amplitudes, the groove size of 5 mm is employed. At last, the overall visible sizes of the optimized ultrasonic vibrator are shown in TABLE 2.

C. TEST EXPERIMENT

Considering the function of rotating polishing angle, the external structure of the device is designed. TDUP system is shown in Fig. 6, the shell is connected with the flange to isolate external interference ensuring the operation of the ultrasonic device stably. The turntable adopts double-nuts structure to make device have a rotary function at arbitrary angle and realizes the partial height adjustment. The polishing tool is detachable and a wrench position is made on the transformer for the purpose of fixing the nut tightly when the polishing tool is replaced. Accordingly, different polishing

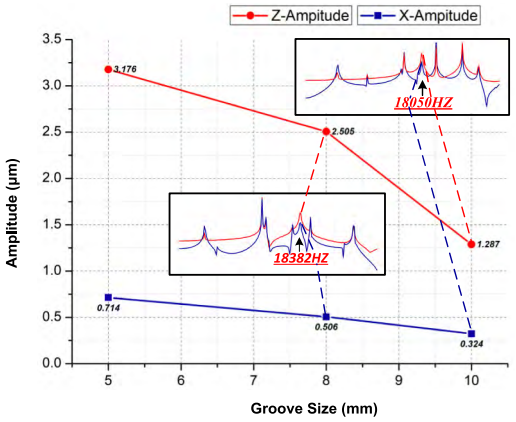

FIGURE 5. Influence of the groove sizes on ultrasonic amplitudes and resonance frequency in the simulation.

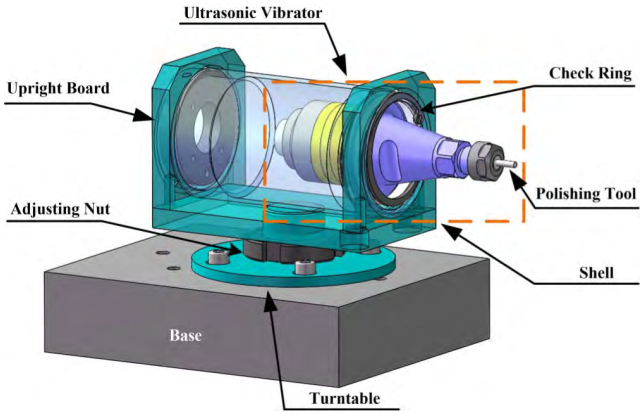

FIGURE 6. Schematic diagram of external structures of device.

tools can be selected when facing different surface structure to increase the polishing flexibility of the device.

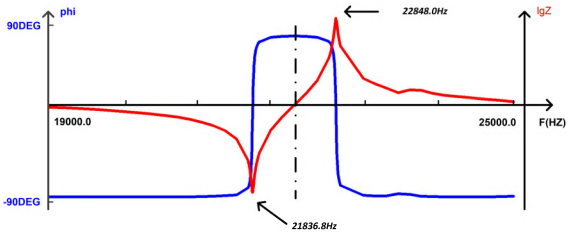

FIGURE 7. Impedance test result of the ultrasonic vibrator.

Test experiments are implemented on the fabricated prototype to verify the rationality of the finite element analysis. An impedance analyzer (PV520A) was employed to measure the resonance frequency of longitudinal-bending vibration modes. As shown in Fig.7, the resonance frequency of device is 22848.0Hz, which has difference from the simulation result. The resonance frequency obtained by modal analysis is the ideal frequency, which is affected by assembly and material, and the electrodes are ignored in simulation. The TDUP device proposed in this paper is uncommon that it have the function of replaceable polishing tools which is different from the ultrasonic cutting device that only replace the standard blade. A variety of polishing tools are required during the actual processing to accurately perform polishing. For this reason, the shape and size of the polishing tools cannot be determined precisely during the simulation. In this paper, a straight stick was selected for simplification. The materials, the length and the weight of polishing tools will have a large impact on the actual resonance frequency. Considering of these factors above, the error is acceptable.

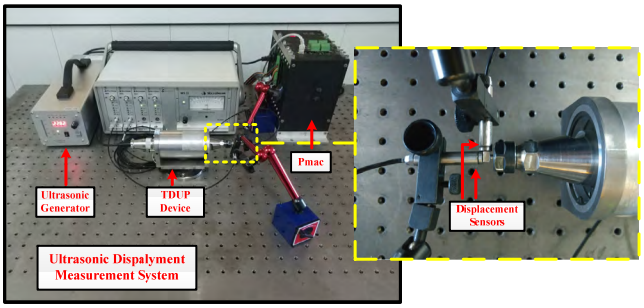

FIGURE 8. Photograph of the test experimental setup for amplitudes.

Fig. 8 shows a photograph of the test experimental setup for amplitudes. The ultrasonic generator sends out AC signals to actuate the PZTs to produce high frequency vibration. Then the displacement signals are collected by capacitive displacement sensor and convert into voltage signals, which are displayed in the multichannel position measurement system. Finally, the voltage signals are input to the PMAC acquisition card and recorded by POWER PMAC IDE software. The ultrasonic system operates at 22.82 kHz with 10% power.

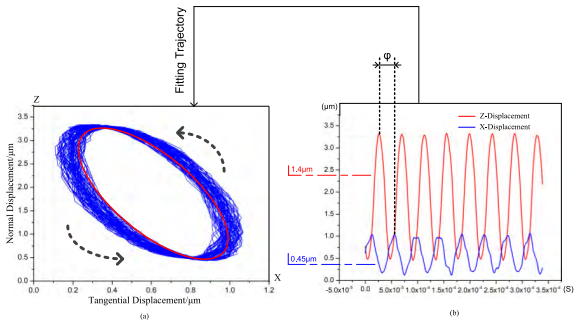

FIGURE 9. Experimental results of amplitudes test and trajectory.

The results of amplitudes tests are shown in Fig. 9. It can be seen that the actual vibration locus is wider than the ideal locus in Fig. 9(a). This is because the small x-direction amplitude of the two-dimensional ultrasonic device is easily affected by environmental disturbances. As can be seen from the Fig. 9(b), the larger Z-direction amplitude has a better sinusoidal curve while the smaller X-direction amplitude curve is not smooth. The arrows in Fig. 9(a) represent the direction of the ellipse trajectory to determine the access point for subsequent modeling. In Fig. 9(b), the maximum

longitudinal and transverse displacement are about 1.4μm and 0.45μm, respectively. The ratio of amplitudes is 3.11. Obviously, there is an error between test results and the simulation. This is mainly due to the magnitude of the applied force in the harmonic response analysis and voltage output power do not correspond. The amplitude of two-dimensional ultrasonic device can increase with the power. The phase difference is about 120 degrees.

Although there are some errors, the test results are generally consistent with the simulation results of the TDUP device which are basically acceptable. The device could achieve the longitudinal- bending ultrasonic vibration driven by single AC signals, which realize the function of rotating machine angle and changing polishing tools under different polishing purposes. The overall design size of half wavelength is adopted in the design to make it have smaller volume. When the preloading force on the nut is large enough, the working stability of the TDUP system can be guaranteed, and there is no obvious heating phenomenon after working for 1 hour.

III. POLISHING MECHANISM

A model was developed to explain the polishing angles arise from the non-determinacy of machining and how to influence the surface quality on complex structure of biomaterials. Firstly, one single diamond particle is considered in process of developing model and then the force of each diamond particles that actually participate in the polishing process are taken into account. Finally, the model of multiangle polishing mechanism is established. Some assumptions should be given as follows before modeling.

- Diamond particles are assumed to be rigid spheres of the same size.
- The particles are invariable in shape during polishing.
- The ultrasonic vibration maintains a stable working state.

A. KINEMATICS ANALYSIS OF DIAMOND PARTICLE

The movement trajectory of one diamond particle in TDUP is not only a combination of normal (Z-direction) and tangential (X-direction) direction of ultrasonic vibration, but also feed motion and spindle rotation. The purpose of model is to investigate the multiangle polishing mechanism in one period. Therefore, tangential feed and spindle rotation are neglected in kinematics analysis. The ideal motion trajectory of the diamond particle relative to the workpiece in TDUP can be expressed as:

$$\begin{cases} \mathrm{X} = B\sin(2\pi ft + \varphi) \\ Z = A\sin 2\pi ft \end{cases} \tag{1}$$

where f is the ultrasonic vibration frequency, Hz; A and B are ultrasonic vibration amplitudes, μm; φ is phase difference, *deg*; and t is the polishing time, s. Ultrasonic vibration in the X- and Z-direction are fitted into an elliptical trajectory. The conversion coordinate is calculated by rotation matrix as follow;

$$\begin{bmatrix} x \\ z \end{bmatrix} = \begin{bmatrix} \cos\theta & \sin\theta \\ -\sin\theta & \cos\theta \end{bmatrix} \begin{bmatrix} x_1 \\ z_1 \end{bmatrix} \tag{2}$$

The movement trajectory of one diamond particle can be described accurately by the oblique ellipse plane equation, which is obtained by substituting the conversion coordinate into the original elliptical equation as;

$$\frac{(z_1\sin\theta + x_1\cos\theta)^2}{B^2} + \frac{(z_1\cos\theta - x_1\sin\theta)^2}{A^2} - \frac{2(z_1\sin\theta + x_1\cos\theta)(z_1\cos\theta - x_1\sin\theta)}{AB}\cos\varphi = \sin^2\varphi \tag{3}$$

where θ is polishing angle, *deg*; x_1 and z_1 are conversion coordinates after rotating. In TDUP, the polishing tool drives the particle to move periodically along the elliptical trajectory and it enters the workpiece at point A, which is graphically displayed in Fig.10. The positive normal kinetic energy is exhausted when the particle arrives at point B, which is the lowest point. At the same time, it keeps up motion under the tangential kinetic energy.

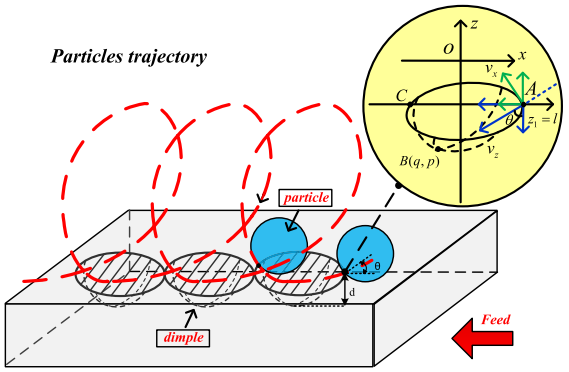

FIGURE 10. Schematic diagram of two-dimensional ultrasonic polishing.

The horizontal plane of workpiece is expressed as $Z = l$ that is plugged into (3); (4) shown at the bottom of the next page.

Both the coordinate of point A and point C can be calculated by solving for x_1 in (4) as below A and C, shown at the bottom of the next page, where $\eta = A^2\cos^2\theta + B^2\sin^2\theta + 2AB\cos\varphi\sin\theta\cos\theta$

B. FORCE ANALYSIS

An equivalent solution is adopted to calculate the velocity of the access point because the velocity is difficult to be calculated in oblique ellipse plane equation, which has no influence on the accuracy of the velocity. In this paper, the equivalent access point that is set as the point M will be emphatically discussed. Fig. 11 demonstrates the transformation process of ellipse in modeling. The actual access point A on oblique elliptical trajectory is converted back to the original position to obtain the equivalent access point M. The positions of two points on the ellipse are the same, with the same velocity and

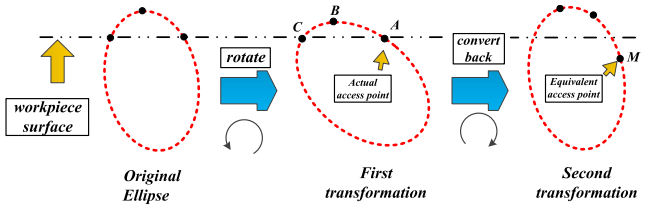

FIGURE 11. Schematic diagram of equivalent coordinate transformation.

the same acceleration. By calculating the velocity of the point M on the original ellipse, the velocity of diamond particle entering the workpiece can be calculated simply.

The equivalent point M can be expressed as;

$$\mathrm{M}: (l\sin\theta + \gamma\cos\theta, l\cos\theta - \gamma\sin\theta)$$

γ is defined as the abscissa value of the point A for convenience. It is primitive to obtain the X-equivalent time t_x and Z-equivalent time t_z because of the known X-displacement and Z-displacement. Then these values of times are substituted into the corresponding velocity equations. Finally, the velocity of access point can be acquired as;

$$\begin{cases} v_x = 2\pi f\ (l\sin\theta + \gamma\cos\theta) \\ v_z = 2\pi f\ (l\cos\theta - \gamma\sin\theta) \end{cases} \tag{5}$$

As shown in Fig.10, the normal component of v_x and v_z are synthesized to a vector perpendicular to the workpiece.

$$v_{res} = 2\pi f\left(l\cos^2\theta - l\sin^2\theta - 2\gamma\sin\theta\cos\theta\right) \tag{6}$$

The workpiece is subjected to the normal force during the process of TDUP and intermittent normal ultrasonic vibration cause the diamond particle to separate from the workpiece. The normal force has been reducing gradually as the velocity decreasing until the diamond particle leaves away from the workpiece. The depth of indentation is defined as the distance from the contact plane to the bottom of dimple. Based on the law of conservation of momentum, the maximum $F(z_1)$ is evaluated through the normal velocity and the quality of the particle.

$$\int_0^d F\Delta z_1 = \frac{mv^2}{2} \tag{7}$$

From the deduction above, substituting (6) into (7), the model of the normal force of one diamond particle is built as;

$$\begin{aligned} F &= \frac{2\pi\rho r^3 v^2}{3(p-l)} \\ &= \frac{8\pi^3 r^3 f^2 \rho\left[l\cos^2\theta - l\sin^2\theta - 2\gamma\sin\theta\cos\theta\right]^2}{3(p-l)} \end{aligned} \tag{8}$$

where ρ is density of the diamond particle, $g/\mu m^3$; r is the radius of the particle, μm; d is indentation depth μm; p is the maximum value of the Z-axis of oblique ellipse, μm. Equation (3) is derived with respect to x_1 for solving the coordinate of point B. The result is given as;

$$\begin{aligned} z_1' = &-\frac{(A^2\cos^2\theta + B^2\sin^2\theta + 2AB\cos\varphi\sin\theta\cos\theta)x_1}{(A^2\sin^2\theta + B^2\cos^2\theta - 2AB\cos\varphi\sin\theta\cos\theta)z_1} \\ &\times\frac{+\left[(A^2-B^2)\sin\theta\cos\theta + AB\cos\varphi\left(\sin^2\theta - \cos^2\theta\right)\right]z_1}{+\left[(A^2-B^2)\sin\theta\cos\theta + AB\cos\varphi\left(\sin^2\theta - \cos^2\theta\right)\right]x_1} \end{aligned} \tag{9}$$

where z_1' is equal to zero, owing to the relationship between x_1 and z_1, the coordinate can be derived as B: (x_1, z_1), shown at the bottom of this page.

Accordingly, the p value can be obtained. All of the factors are known in the model of the normal force of a diamond particle.

C. TOTAL NORMAL FORCE

The force condition of single diamond particle in TDUP was mentioned above. However, during the actual polishing machining, it is impossible to have just one diamond particle. Instead, a number of diamond particles have combined action. In this paper, a spherical polishing tool adhered with diamond particles was used. Tiny elastic deformation occurs when the tool contacts the workpiece. The hertz contact theory is employed in this model [30]. And the following equation represents the radius of contact area.

$$R_0 = \left[\frac{3}{4}R\left(\frac{1-v_1^2}{E_1} + \frac{1-v_2^2}{E_2}\right)F\right]^{\frac{1}{3}} \tag{10}$$

$$\left(x_1^2, 2lx_1, l^2\right)\begin{pmatrix} A^2\cos^2\theta + B^2\sin^2\theta + 2AB\cos\varphi\sin\theta\cos\theta \\ A^2\sin\theta\cos\theta - B^2\sin\theta\cos\theta + AB\cos\varphi\sin^2\theta - AB\cos\varphi\cos^2\theta \\ A^2\sin^2\theta + B^2\cos^2\theta - 2AB\cos\varphi\sin\theta\cos\theta \end{pmatrix} = \sin^2\varphi A^2B^2 \tag{4}$$

$$A: \left(\frac{l\left[\left(B^2-A^2\right)\sin\theta\cos\theta + AB\cos\varphi\left(\cos^2\theta - \sin^2\theta\right)\right] + AB\sqrt{-\cos^2\varphi\left(4l^2\sin^2\theta\cos^2\theta - l^2 + \eta\right) + \eta - l^2}}{A^2\cos^2\theta + B^2\sin^2\theta + 2AB\cos\varphi\sin\theta\cos\theta}, l\right)$$

$$C: \left(\frac{l\left[\left(B^2-A^2\right)\sin\theta\cos\theta + AB\cos\varphi\left(\cos^2\theta - \sin^2\theta\right)\right] - AB\sqrt{-\cos^2\varphi\left(4l^2\sin^2\theta\cos^2\theta - l^2 + \eta\right) + \eta - l^2}}{A^2\cos^2\theta + B^2\sin^2\theta + 2AB\cos\varphi\sin\theta\cos\theta}, l\right)$$

where R_0 is the radius of contact area, μm; Poisson's ratio v_1, v_2; Young's modulus E_1, E_2;

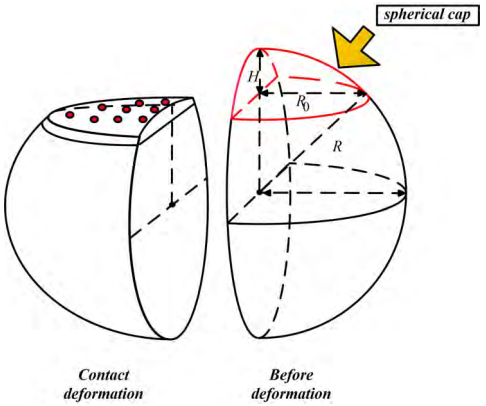

FIGURE 12. Schematic diagram of morphology of polishing tool before and after deformation.

Fig. 12 shows the morphology of polishing tool before and after the elastic deformation. The spherical cap is extruded into a slightly convex surface. Therefore, the number of diamond particles adhering to the surface of spherical cap can be approximately regarded as the number of diamond particles actually participating in polishing. According to the formula of superficial area of spherical cap, *Na* is calculated, as follow;

$$N_a = 2\pi R_0 \cdot H \cdot c \tag{11}$$

where c is the number of diamond particles per unit area of polishing tool.

In conclusion, the total normal force model has been developed in TDUP.

$$F_t = F_s \cdot 2\pi \left[\frac{3}{4}R\left(\frac{1-v_1^2}{E_1}+\frac{1-v_2^2}{E_2}\right)F\right]^{\frac{1}{3}} \cdot\left(R-\sqrt{R^2-\left[\frac{3}{4}R\left(\frac{1-v_1^2}{E_1}+\frac{1-v_2^2}{E_2}\right)F\right]^{\frac{2}{3}}}\right)\cdot c \tag{12}$$

The model can be employed to predict the normal force in TDUP. It can be seen from (8) that the normal force is proportional to the normal velocity. In the next chapter, we will discuss the coincidence of the model concretely and intuitively by the normal velocity.

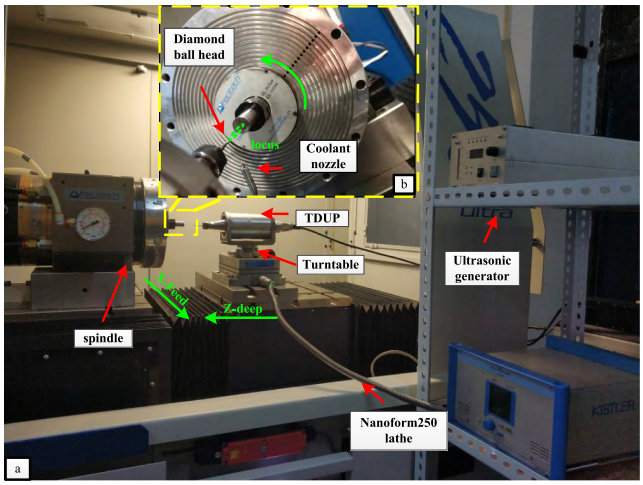

FIGURE 13. Photograph of the setup for micro-polishing.

IV. EXPERIMENTS

A. EXPERIMENTAL DETAILS

Polishing experiments were conducted to verify the performance and effectiveness of proposed device. Fig. 13(a) is the photograph of the ultrasonic polishing. An ultra-precision machine tool (nanoform250, USA) was used and ultrasonic device was installed in the guide of lathe, facing the spindle in which the workpiece was installed by the vacuum chuck. 20K Ultrasonic Generator supplied the ultrasonic vibrator for energy. As shown in Fig. 13(b), the position relationship between the polishing tool and the workpiece is introduced. These experiments were carried out on the end face of Ti6Al4V sample with strength of 1.012GPa and the size of the specimen was φ12.7mm. All specimens were dried out after being washed down for 5 minutes with acetone and ethanol. Polishing experiments were divided into two groups. The first group was carried out to survey the machining performance of the proposed device on the Ti6Al4V surface. Cylindrical polishing tool with the granularity of 3000 was applied because uniform diamond particles participated in the polishing area that is benefited for distinguishing the polishing behavior. In the second group, four different polishing angles (10°, 20°, 30°, 40°) were selected to explore how the actual quality of biomaterials workpiece surface was affected. A spherical polishing tool with the granularity of 300 was used, which could satisfy all of the polishing angle conditions. Meanwhile, coolant was used for real-time cooling. The experimental conditions were listed in TABLE 3 in detail.

$$\mathrm{B}:(x_1,z_1)=\left(-\frac{\left[\left(A^2-B^2\right)\sin\theta\cos\theta+AB\cos\varphi\left(\sin^2\theta-\cos^2\theta\right)\right]\sin\varphi}{\sqrt{\left[1-\cos^2\varphi\left(\sin^4\theta+\cos^4\theta\right)\right]\left(A^2\cos^2\theta+B^2\sin^2\theta+2AB\cos\varphi\sin\theta\cos\theta\right)}},\frac{\left(A^2\cos^2\theta+B^2\sin^2\theta+2AB\cos\varphi\sin\theta\cos\theta\right)\sin\varphi}{\sqrt{\left[1-\cos^2\varphi\left(\sin^4\theta+\cos^4\theta\right)\right]\left(A^2\cos^2\theta+B^2\sin^2\theta+2AB\cos\varphi\sin\theta\cos\theta\right)}}\right)$$

TABLE 3. Parameters of polishing experiments

Symbol	Experimental conditions 1	Experimental conditions 2
Angles	0°	10°, 20°, 30°, 40°
Materials	Ti6Al4V	Ti6Al4V
Spindle speed	1500rpm	1500rpm
Feed rate	60mm/min	60mm/min
Depth of cut	5μm, 1μm/min	5μm, 1μm/min
Ultrasonic vibration	Yes/no	Yes
Frequency	22570Hz	22570Hz
Amplitudes	X 0.45μm, Z 1.4μm	X 0.45μm, Z 1.4μm
Polishing tool	Cylindrical tool	Spherical tool

B. RESULTS AND DISCUSSION

The surface roughness and profile were measured by using a white-light interferometer (ZygoNewview, USA). Fig. 14(a) exhibits the surface morphology of the titanium alloy at 166.87μm micron scale without ultrasonic vibration. The workpiece surface is coarse, accompanied by a mass of burrs. The maximum peak value is 2.799μm and the surface smoothness is poor whose surface roughness is 235 nm. However, fig. 14(b) shows the surface morphology of the workpiece at 166.87μm micron scale when applying ultrasonic vibration. Its maximum peak value drops to 1.313μm and the surface roughness is 146 nm. Those results illustrate that the surface quality of titanium alloy has been improved obviously by adding ultrasonic vibration, which might be attributed to the traditional polishing, unless under specific lubrication, will cause chip adhesion [31]. Besides, with the merits of ultrasonic machining, the force will decrease and tiny debris will be quickly removed. Thus, the surface roughness is reduced. Furthermore, the polished surface exists obvious continuous vibration structure. Not only does the ultrasonic vibration remove the burrs on the surface and greatly improve the smoothness of the surface, but this structure may be more suitable for cell attachment and manifests better cell metabolic responses in implanted materials [32]. Meanwhile, both relatively high surface roughness and surface vibration structure may be beneficial to improve the bone bonding ability [33]. To evaluate the polishing performance of the proposed device better. Fig. 14(c) presents the surface morphology of the workpiece at 834.37μm micron scale with ultrasonic vibration. It is observed that the surface morphology maintains a continuous vibration structure with a maximum peak value of 1.598μm and a surface roughness of 140 nanometers at the enlarged observation scale of 5 times. According to the analysis above, it is indicated that the addition of two-dimensional ultrasonic vibration in polishing has an enormous influence on the surface morphology of titanium alloy. The surface roughness and maximum peak value decrease significantly whether observation scales. It accounts for that the proposed device can effectively improve the surface quality, form continuous vibration structure which may facilitate the attachment of human tissue, and give it potential to produce excellent surgical implants products.

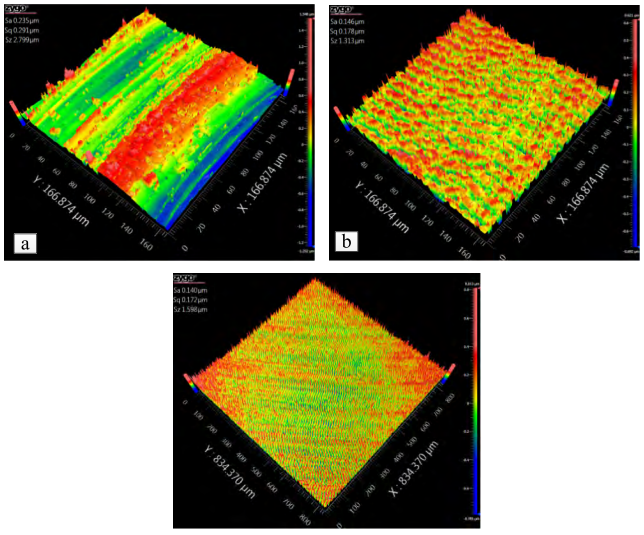

FIGURE 14. Surface morphology (a) non-ultrasonic vibration polishing (b) ultrasonic vibration polishing and (c) ultrasonic vibration polishing at 5 times observation scale.

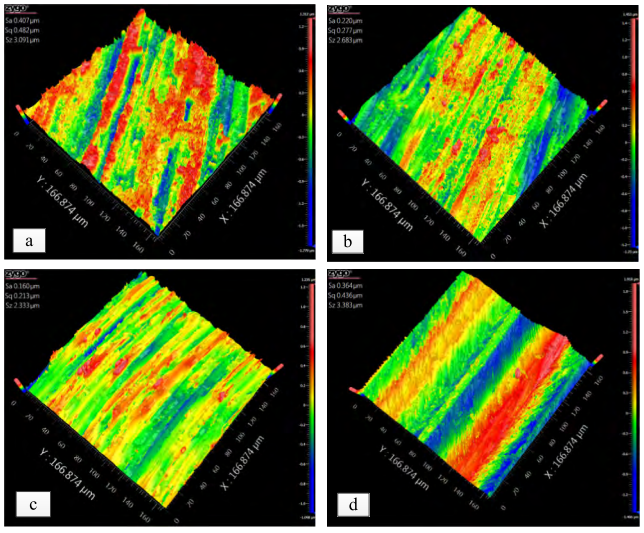

FIGURE 15. Surface morphology of multiangle (a) 10° (b) 20° (c) 30° (d) 40°.

The results for multiangle experiments are depicted in Fig.15. Compared with Fig.14 (b), there are irregular gully marks instead of regular vibration structure on the surface at the polishing angle of 10 degrees. The reason is that the coarse spherical polishing tools were adopted in the experiments and the extended particles inevitably destroy the surface morphology, which indicated the granularity of polishing tool has a great influence on the surface quality. The surface roughness is 407nm and the maximum is 3.091μm in the Fig.15 (a). The surface morphology of workpiece at the polishing angle

of 20 degrees is shown in Fig. 15(b). The gully marks become more distinct. That is because the normal velocity perpendicular to the workpiece surface and the normal force decrease when the polishing angle is changed. Accordingly, the diamond particles alleviate the damage to the workpiece surface vibration structure. The surface roughness is 220nm and the maximum is 2.683μm. In Fig. 15(c), the surface of titanium alloy emerges more obvious gully marks at the polishing angle of 30 degrees, which is due to the further reduction of normal velocity. The surface roughness is 160nm and the maximum is 2.333μm. However, in Fig. 15(d), wider grooves can be conspicuously seen instead of gully marks on the surface morphology at the polishing angle of 40 degrees. Probably because the normal velocity has been reversed at the angle of 40 degrees and the actual effect of polishing is the friction effect of the tangential velocity. Meanwhile, the reverse of normal velocity recedes the removal rate leading to the surface roughness increases. The surface morphology produced by the friction effect is obviously different from that produced by the normal velocity. The roughness is 364nm and the maximum is 3.383μm. These results indicate that the surface quality of the workpiece is affected by the changing of polishing angle. The surface roughness decreases and the normal velocity gradually reducing with the polishing angle increasing. However, the surface roughness increases and the surface morphology of the workpiece changes from gully marks to grooves when the velocity gradually reverses causing the direction of the main force to change.

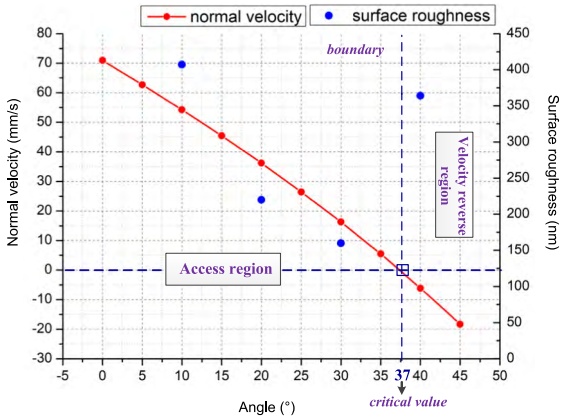

FIGURE 16. Graph of comparing the results of experiments with model trend.

A graph of relationship between the angles and the normal velocity is calculated by the model at the third chapter which is shown in Fig. 16. As can be seen from the graph, the normal velocity decreases with the increase of the polishing angle in all regions. When the polishing angle increases to about 37 degrees (the critical value), the normal velocity approaches zero. The area on the left side of the boundary is the access region. On the other side, the area is the velocity reverse region. In the access region the velocity and the roughness decrease with the increase of polishing angle. However, in the velocity reverse region, the reverse velocity increases and the roughness raises sharply as the increase of angle. The reason may be due to the transformation of polishing mechanism. The normal force, which plays a decisive role, disappears and may be replaced by tangential scraping in the velocity reverse region. The critical value is not a fixed value under the influence of pressing depth, amplitude and frequency, etc. The significance of modeling is to find the critical value under different machining parameters to guide the polishing. The analysis results show that the polishing mechanism model agrees with the experimental results well.

V. CONCLUSION

In conclusion, a new ultrasonic vibration device was designed and the structural parameters were optimized through finite element analysis. Polishing experiments had been implemented to prove that the device has great potentials to satisfy the surface quality of biomaterials and polishing angles influence the surface roughness obviously. The main conclusions of this paper can be summarized below:

1. The ultrasonic device with asymmetric transformer in this paper is driven by single AC signals to generate the elliptical motion. The 5mm half-cylinder groove can improve the resonance frequency and amplitudes with the help of finite element analysis so that the device can work well stably. Then, the experimental results show that the longitudinal amplitude of the device is 1.4μm and the transverse amplitude of the device is 0.45μm at 10% power. The phase difference is about 120 degrees and the ultrasonic resonance frequency is 22848.0 Hz. Considering a few practical influence factors, the whole design can be accepted in spite of existing deviations.

2. The results of polishing experiments reveal that the surface of titanium alloy appears regular and continuous vibration structure when the device employs fine electroplated diamond tool, which remarkably improves the smoothness. The surface roughness is reduced to 140nm compared with 235nm without ultrasonic vibration. Two-dimensional ultrasonic vibration can significantly improve the surface morphology and surface quality of titanium alloy.

3. The results of multiangle experiments show that different polishing angles influence the surface roughness obviously. The surface roughness decreases from 407nm to 160nm when the polishing angle increases from 10 to 30 degrees. The normal velocity reverses when the angle increasing to the critical value in which the main motion of polishing transform into tangential scraping and the polishing mechanism is changed. The surface roughness increases as well. These results are proved in accordance with the model of multiangle polishing mechanism properly.

REFERENCES

[1] M. Vallet-Regí, "Revisiting ceramics for medical applications," *Dalton Trans.*, no. 44, pp. 5211–5220, Oct. 2006.

[2] W. Qu, K. Wang, M. H. Miller, Y. Huang, and A. Chandra, "Using vibration-assisted grinding to reduce subsurface damage," *Precis. Eng.*, vol. 24, no. 4, pp. 329–337, Oct. 2000.

[3] J. Wang, P. Feng, J. Zhang, and P. Guo, "Experimental study on vibration stability in rotary ultrasonic machining of ceramic matrix composites: Cutting force variation at hole entrance," *Ceramics Int.*, vol. 44, no. 12, pp. 14386–14392, Aug. 2018.
[4] J. Wang, J. Zhang, P. Feng, and G. Ping, "Damage formation and suppression in rotary ultrasonic machining of hard and brittle materials: A critical review," *Ceramics Int.*, vol. 44, no. 2, pp. 1227–1239, 2018.
[5] R. Kurniawan, S. T. Kumaran, S. Ali, D. A. Nurcahyaningsih, G. Kiswanto, and T. J. Ko, "Experimental and analytical study of ultrasonic elliptical vibration cutting on AISI 1045 for sustainable machining of round-shaped microgroove pattern," *Int. J. Adv. Manuf. Technol.*, vol. 98, nos. 5–8, pp. 2031–2055, Sep. 2018.
[6] X. Zhang, H. Sui, D. Zhang, and X. Jiang, "Study on the separation effect of high-speed ultrasonic vibration cutting," *Ultrasonics*, vol. 87, pp. 166–181, Jul. 2018.
[7] Y. Yang and P. Guo, "Global tool path optimization of high-resolution image reproduction in ultrasonic modulation cutting for structural coloration," *Int. J. Mach. Tools Manuf.*, vol. 138, pp. 14–26, Mar. 2019.
[8] T. Yu, X. Yang, J. An, X. Yu, and J. Zhao, "Material removal mechanism of two-dimensional ultrasonic vibration assisted polishing Inconel718 nickel-based alloy," *Int. J. Adv. Manuf. Technol.*, vol. 96, nos. 1–4, pp. 657–667, Apr. 2018.
[9] T. Yu, Z. Wang, X. Guo, P. Xu, J. Zhao, and L. Chen, "Effect of ultrasonic vibration on polishing monocrystalline silicon: Surface quality and material removal rate," *Int. J. Adv. Manuf. Technol.*, pp. 1–11, Apr. 2019.
[10] W. Xu, X. Lu, G. Pan, Y. Lei, and J. Luo, "Ultrasonic flexural vibration assisted chemical mechanical polishing for sapphire substrate," *Appl. Surf. Sci.*, vol. 256, no. 12, pp. 3936–3940, Apr. 2010.
[11] H. Suzuki, T. Moriwaki, T. Okino, and Y. Ando, "Development of ultrasonic vibration assisted polishing machine for micro aspheric die and mold," *CIRP Ann.*, vol. 55, no. 1, pp. 385–388, 2006.
[12] H. Suzuki, S. Hamada, T. Okino, M. Kondo, Y. Yamagata, and T. Higuchi, "Ultraprecision finishing of micro-aspheric surface by ultrasonic two-axis vibration assisted polishing," *CIRP Annals*, vol. 59, no. 1, pp. 347–350, 2010.
[13] Q. Zhao, Z. Sun, and B. Guo, "Material removal mechanism in ultrasonic vibration assisted polishing of micro cylindrical surface on SiC," *Int. J. Mach. Tools Manuf.*, vol. 103, pp. 28–39, Apr. 2016.
[14] H. Hong and K. Kuo, "Fundamental study of ultrasonic polishing of model steel," *Int. J. Mach. Tool. Manu.*, vol. 42, no. 1, pp. 7–13, Jan. 2002.
[15] D. Jia, C. Li, Y. Zhang, M. Yang, X. Zhang, R. Li, and H. Ji, "Experimental evaluation of surface topographies of NMQL grinding ZrO_2 ceramics combining multiangle ultrasonic vibration," *Int. J. Adv. Manuf. Technol.*, vol. 100, nos. 1–4, pp. 457–473, Jan. 2019.
[16] K. Zheng, W. Liao, Q. Dong, and L. Sun, "Friction and wear on titanium alloy surface machined by ultrasonic vibration-assisted milling," *J. Brazilian Soc. Mech. Sci. Eng.*, vol. 40, p. 411, Sep. 2018.
[17] X. Xiao, K. Zheng, and W. Liao, "Theoretical model for cutting force in rotary ultrasonic milling of dental zirconia ceramics," *Int. J. Adv. Manuf. Technol.*, vol. 75, nos. 9–12, pp. 1263–1277, Dec. 2014.
[18] J. Pujana, A. Rivero, A. Celaya, and L. N. L. de Lacalle, "Analysis of ultrasonic-assisted drilling of Ti6Al4V," *Int. J. Mach. Tools Manuf.*, vol. 49, no. 6, pp. 500–508, May 2009.
[19] T. Moriwaki and E. Shamoto, "Ultrasonic elliptical vibration cutting," *CIRP Ann.*, vol. 44, no. 1, pp. 31–34, 1995.
[20] D. Deligianni, N. Katsala, S. Ladas, D. Sotiropoulou, J. Amedee, and Y. F. Missirlis, "Effect of surface roughness of the titanium alloy Ti-6Al-4V on human bone marrow cell response and on protein adsorption," *Biomaterials*, vol. 22, no. 11, pp. 1241–1251, Jun. 2001.
[21] X. Li and D. Zhang, "Ultrasonic elliptical vibration transducer driven by single actuator and its application in precision cutting," *J. Mater. Process. Technol.*, vol. 180, nos. 1–3, pp. 91–95, Dec. 2006.
[22] Z. Yin, Y. Fu, J. Xu, H. Li, Z. Cao, and Y. Chen, "A novel single driven ultrasonic elliptical vibration cutting device," *Int. J. Adv. Manuf. Technol.*, vol. 90, nos. 9–12, pp. 3289–3300, Jun. 2017.
[23] P. Guo and K. F. Ehmann, "An analysis of the surface generation mechanics of the elliptical vibration texturing process," *Int. J. Mach. Tools Manuf.*, vol. 64, pp. 85–95, Jan. 2013.
[24] Z. Haidong, L. Shuguang, Z. Ping, and K. Di, "Process modeling study of the ultrasonic elliptical vibration cutting of Inconel 718," *Int. J. Adv. Manuf. Technol.*, vol. 92, nos. 5–8, pp. 2055–2068, Sep. 2017.
[25] H. Al-Budairi, M. Lucas, and P. Harkness, "A design approach for longitudinal-torsional ultrasonic transducers," *Sens. Actuators A, Phys.*, vol. 198, pp. 99–106, Aug. 2013.
[26] W. Huang, D. Yu, M. Zhang, F. Ye, and J. Yao, "Analytical design method of a device for ultrasonic elliptical vibration cutting," *J. Acoust. Soc. Amer.*, vol. 141, no. 2, p. 1238, Feb. 2017.
[27] D. Bai, Q. Quan, Y. Wang, D. Tang, and Z. Deng, "A longitudinal & longitudinal-torsional vibration actuator for rotary-percussive ultrasonic planetary drills," *Adv. Space. Res.*, vol. 63, no. 2, pp. 1065–1072, Jan. 2019.
[28] H. Ni, Y. Wang, H. Gong, L. Pan, Z. Li, and D. Wang, "A novel free-form transducer for the ultra-precision diamond cutting of die steel," *Int. J. Adv. Manuf. Technol.*, vol. 95, nos. 5–8, pp. 2185–2192, Mar. 2018.
[29] R. Tan, X. Zhao, X. Zou, and T. Sun, "A novel ultrasonic elliptical vibration cutting device based on a sandwiched and symmetrical structure," *Int. J. Adv. Manuf. Technol.*, vol. 97, nos. 1–4, pp. 1397–1406, Jul. 2018.
[30] K. L. Johnson, K. Kendall, and A. D. Roberts, "Surface energy and the contact of elastic solids," *Proc. Roy. Soc. A. Math. Phys. Eng. Sci.*, vol. 324, no. 1558, pp. 301–313, Sep. 1971.
[31] M. G. Nik, M. R. Movahhedy, and J. Akbari, "Ultrasonic-assisted grinding of Ti6Al4V alloy," in *Proc. CIRP Conf. High Perform. Cutting*, vol. 1, Jul. 2012, pp. 353–358. doi: 10.1016/j.procir.2012.04.063.
[32] W.-C. Chen, Y.-S. Chen, C.-L. Ko, Y. Lin, T.-H. Kuo, and H.-N. Kuo, "Interaction of progenitor bone cells with different surface modifications of titanium implant," *Mater. Sci. Eng. C*, vol. 37, pp. 305–313, Apr. 2014.
[33] A. E. Medvedev, A. Neumann, H. P. Ng, R. Lapovok, C. Kasper, T. C. Lowe, V. N. Anumalasetty, and Y. Estrin, "Combined effect of grain refinement and surface modification of pure titanium on the attachment of mesenchymal stem cells and osteoblast-like SaOS-2 cells," *Mater. Sci. Eng. C*, vol. 71, pp. 483–497, Feb. 2017.

JIEQIONG LIN received the M.S. degree from the Changchun University of Technology, Changchun, China, in 2001, and the Ph.D. degree in mechanical manufacturing from Jilin University. Changchun, in 2005. She is currently a Professor with the School of Mechatronic Engineering, Changchun University of Technology. She is also an active Researcher and her research interests include industry-related and applied research in ultra-precision machining, large-area laser processing, precision polishing, and error compensation.

HAO LU was born in Liaoning, China, in 1994. He received the B.S. degree from the Shenyang University of Technology, Shenyang, China, in 2017. He is currently pursuing the M.S. degree with the Department of Mechanical Engineering, Changchun University of Technology. His research interests include precision polishing on biomaterials and design of resonant vibration-assisted.

YAN GU received the B.E. and M.S. degrees in mechanical engineering from the Changchun University of Technology, Changchun, China, in 2004 and 2009, respectively, and the Ph.D. degree in mechanical manufacturing from Jilin University, Changchun, in 2014. He is currently a Lecturer with the School of Mechatronic Engineering, Changchun University of Technology. His research interests include ultra-precision machining, non-resonant vibration-assisted device design, and nano-printing.

XIAOQIN ZHOU received the M.S. degree from Jilin University, in 1990, and the Ph.D. degree in mechanical manufacturing from Jilin University, in 1998. He currently serves as the Vice-Dean of the College of Mechanical Science and Engineering, and he is also in charge of mechanical engineering. His current research interests include ultra-precision manufacturing, intelligent manufacturing, automotive key parts manufacturing, complex optical manufacturing, intelligent optical and mechanical systems, micro nano-ultra-precision motion control, metal materials manufacturing, and superstructure materials.

CHENGLEI XIN was born in Shandong, China, in 1996. He received the B.S. degree in mechanical engineering from Shandong Agricultural Engineering University, Jinan, China, in 2018. He is currently pursuing the M.S. degree in mechanical engineering from the Changchun University of Technology. His research interests include ultrasonic machining, and interface science and application.

MINGSHUO KANG was born in Jilin, China, in 1995. He is currently pursuing the B.S. degree with the Department of Mechanical Engineering, Changchun University of Technology. His research interests include precision polishing and finite element simulation.

XINYU CANG was born in Shandong, China, in 1998. He is currently pursuing the B.S. degree with the Changchun University of Technology. His research interests include precision polishing and dynamics simulation.